

Chiral smectic transition phases appearing near the electric-field-induced phase transition observed by resonant microbeam x-ray scattering

Atsuo Iida,¹ Isa Nishiyama,² and Yoichi Takanishi³

¹*Photon Factory, Institute of Materials Structure Science, High Energy Accelerator Research Organization, 1-1 Oho Tsukuba, Ibaraki 305-0801, Japan*

²*DIC Corporation, Komuro, Ina-machi, Kitaadachi-gun, Saitama, 362-8577, Japan*

³*Department of Physics, Faculty of Science, Kyoto University, Kitashirakawa-oiwake, Sakyo-ku, Kyoto 606-8502, Japan*

(Received 29 October 2013; published 10 March 2014)

The electric-field-induced phase transition of a chiral liquid crystal containing Br revealed a transition phase between the three-layer periodicity ferroelectric phase and the synclinc ferroelectric phase in the electric field versus temperature phase diagram. Resonant x-ray scattering from the transition phase showed a diffuse streak or spotty weak reflections, which were composed of strong $m/3$ -order (where $m = 1$ and 2) reflections and other weak peaks. The spotty reflections were found to be related to a 12-layer periodicity phase with a weak contribution from the 15-layer periodicity. An x-ray intensity analysis based on the Ising model suggested that the 12-layer periodicity phase was composed of two three-layer ferroelectric blocks and six synclinc layers. This model indicated that, in the transition phase, the three-layer ferroelectric molecular configuration gradually changed to the synclinc configuration. The diffuse streak appearing around $m/3$ -order reflections near the field-induced transition from the four-layer periodicity phase to the synclinc ferroelectric phase is also discussed.

DOI: [10.1103/PhysRevE.89.032503](https://doi.org/10.1103/PhysRevE.89.032503)

PACS number(s): 61.30.Eb, 61.30.Gd, 64.70.M–

I. INTRODUCTION

Chiral smectic- C (tilted) liquid crystals are characterized by a one-dimensional layer structure and an average molecular orientation tilted from the layer normal [1]. The molecular tilt direction (the director) between adjacent layers characterizes various phases in the chiral smectic- C phases, such as ferroelectric, antiferroelectric, and ferroelectric phases. In the ferroelectric phase [$\text{Sm-C}^*(q_T = 1)$, where $q_T = [F]/([F] + [A])$, and $[F]$ and $[A]$ are the numbers of synclinc and anticlinc orderings in a unit periodicity, respectively [2,3]] and in the antiferroelectric phase [$\text{Sm-C}_A^*(q_T = 0)$] [4], the directors in the adjacent layers are synclinc and anticlinc, respectively.

Though the subphases appearing between the lower-temperature $\text{Sm-C}_A^*(q_T = 0)$ and higher-temperature $\text{Sm-C}^*(q_T = 1)$ phases have been experimentally found [2,5–7] and theoretically described [8,9], the application of resonant x-ray scattering (RXS) to the characterization and differentiation of the subphases has led to the direct confirmation of their structures [10]. These structures are a low-temperature, three-layer periodicity ferroelectric phase [$\text{Sm-C}_A^*(q_T = 1/3)$] and a high-temperature, four-layer periodicity antiferroelectric phase [$\text{Sm-C}_A^*(q_T = 1/2)$] [10–13]. More recently a new smectic phase with six-layer periodicity has been found using RXS between the Sm-C^* and Sm-C_A^* phases by Wang *et al.* [14] and between Sm-C^* and Sm-C_A^* phases by Takanishi *et al.* [15]. These findings caused a discussion [16–20] that was mainly concerned with the nature and origin of the long-range interlayer interactions.

The close relation between the temperature and electric-field-induced phase transition has been shown [2] and the electric field versus temperature (E - T) phase diagram has been studied using tilt angle measurements and conoscopic observations [2,21], dielectric, electro-optic, and pyroelectric measurements [6,22], and, more recently, the birefringence measurements [3,23,24]. RXS measurements made under an

applied electric field were performed for a Se-containing sample with a device cell structure [25], and the phase transitions between the ferroelectric and antiferroelectric four-layer periodicity phases have been directly revealed [26]. However, only a few RXS studies have been conducted on field-induced phase transitions because of the associated experimental difficulties.

RXS satellite reflections due to the orientational configuration of different subphase appear at $q_z/q_0 = l + m[(1/\nu) + \varepsilon]$, where q_z is a scattering vector, $q_0 = 2\pi/d$ (d is a smectic layer spacing) l and m ($m \neq 0$) are integers, ν is the superlattice periodicity and ε is the ratio of the layer spacing and the optical pitch [10,27]. High precision analyses have been carried out for a self-standing film [10–14]. In contrast, the cell device structure is required to investigate the field-induced phase transition together with the effect of an applied electric field on the macroscopic layer structure [25,26].

In this paper, the phase change near a field-induced phase transition is investigated using the RXS technique. To study the field-induced phase transition in detail, the device geometry of a sample cell is used. Furthermore, x-ray microbeams are adopted to accurately determine the analyzing position out of the complicated phase boundary appearing near the field-induced phase change. Combining the use of an x-ray microbeam with the device geometry is an effective technique for investigating the local layer structure at the analyzing position since it reflects the molecular alignment in the device under the applied electric field.

II. EXPERIMENT

The liquid crystal used was a sample of (S,S)-bis-[4'-(1-methylheptyloxycarbonyl)-4-biphenyl] 2-bromoterephthalate which contains a bromine atom in its central core component. A detailed characterization of this chiral smectic liquid crystal was reported previously [28]. The

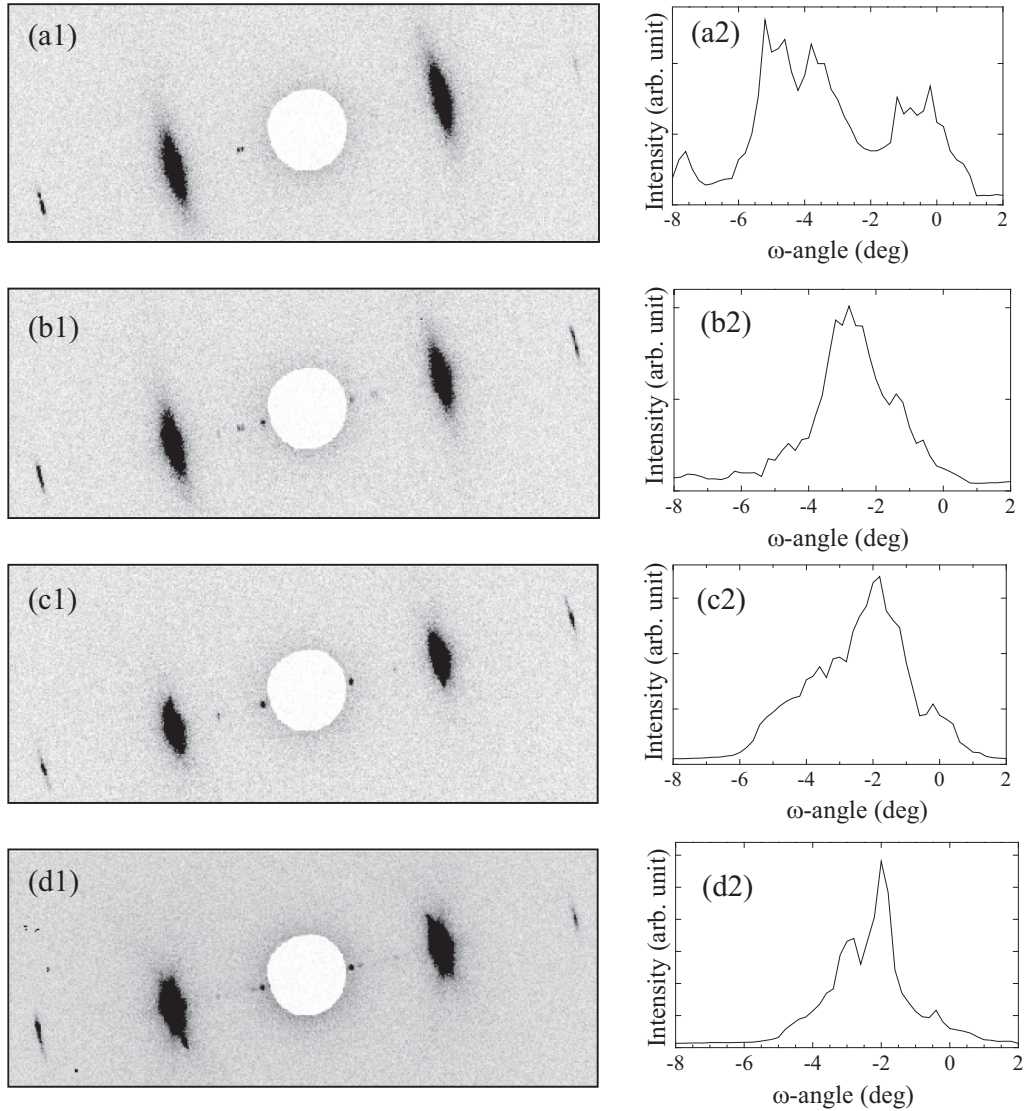


FIG. 1. A series of RXS and ω -angular profiles observed during the experiment at applied fields of (a) ± 20 V, (b) ± 27 V, (c) ± 40 V, and (d) ± 44 V at 140°C . The RXS intensity pattern reveals the large white circles from the direct beam stop at the center, strong first-order and weak second-order layer reflections on both sides, and weak RXS satellites between the white circle and the first-order layer reflection. A few leftmost small spots in (d1) are due to an electronic noise.

sample was sandwiched between $80\text{-}\mu\text{m}$ -thick glass plates coated with indium tin oxide as an electrode and the cell thickness was $25\ \mu\text{m}$. The phase sequence of the material is Iso 201.3°C Sm-A 155°C Sm-C α^* 151.5°C Sm-C* 147°C Sm-C $_A^*$ ($q_T = 1/2$) 145°C Sm-C $_A^*$ ($q_T = 1/3$) 142°C Sm-C $_A^*$ ($q_T = 0$). One side of the glass plate was coated with polyimide and rubbed to obtain a uniform planar domain with a well-defined layer structure. In order to obtain a uniform layer structure, a square-wave electric field (± 40 V maximum) was applied around 140°C , followed by heating to the target phase. The sample cell was mounted on a compact heater, which had small windows of 2 mm in diameter for x-ray transmission. A thermocouple gauge measured the temperature very close to the small window. The temperatures examined were 140, 144, 145.2, and 146°C . The applied electric field was a square-wave form of 20 Hz.

RXS experiments were performed on beam line 4A at the Photon Factory. An x-ray microprobe with a less than $5\text{-}\mu\text{m}$ -square beam was produced by a Kirkpatrick-Baez system in combination with a double crystal monochromator. The sample is positioned at the x-ray focusing point and the layer normal is set approximately horizontally. A vertical rotation axis of the sample was adopted [29]. The incident energy was set to the absorption edge of Br (13.48 keV) for the RXS measurement while it was set below the absorption edge by approximately 14 eV to confirm that the RXS satellite peaks disappear, as RXS only occurs in a quite narrow energy range around the absorption edge. All RXS satellite peaks reported in this paper were confirmed to appear only under resonant conditions. Though the focusing geometry was adopted in this experiment, the horizontal beam divergence was reduced to around 0.5 mrad, which was comparable to the intrinsic angular spread of the local layer structure in the cell, resulting

in a modest angular resolution as well as a reduction of the background x-ray scattering. This also effectively minimized the radiation damage.

A pixel array x-ray detector (Pilatus-100K, DECTRIS) was located 80 cm from the sample. An *in situ* polarizing optical microscope was equipped to monitor the optical response of the sample during the measurement; all photographs shown in this paper were obtained using this microscope. The exposure time ranged from 30 min to 1 h, depending on the experimental condition. The first-order x-ray diffraction intensity as a function of the sample rotation angle (the ω -angular intensity profile) was measured to characterize the local layer structure and to determine the Bragg condition. The RXS intensity was so weak that it was necessary to select a well-aligned layer region to maximize the-signal-to-background (S/B) ratio from the ω -angular intensity profile measurement.

Near the field-induced phase transition, the phase boundary appeared stably due in part to the spatial temperature gradient in the sample (about $0.2^\circ\text{C}/200\ \mu\text{m}$). The microbeam was used to precisely locate the analyzing position even with the temperature gradient and to obtain information on the layer structure.

III. EXPERIMENTAL RESULTS

At 140°C , in the antiferroelectric phase [assigned as $\text{Sm-C}_A^*(q_T = 0)$ without the applied electric field], an optical response to the applied electric field was hardly observed up to an applied field of $\pm 20\ \text{V}$. The ω -angular distribution [Fig. 1(a2)] shows multiple peaks, suggesting a qualitatively vertical chevron structure. The 1/2-order RXS satellite reflections appeared [Fig. 1(a1)] below an applied field of $\pm 20\ \text{V}$, reflecting the two-layer periodicity (defined as Sm-C_{2p} hereafter) anticlinic phase. Figure 1(a1) was obtained at the ω angle of the Bragg condition for the 1/2-order reflection. The splitting of the RXS reflection was due to the long-range helical structure [10,11].

When approaching the field-induced transition between the low-field Sm-C_{2p} (Sm-C_A^*) and high-field three-layer periodicity (defined as Sm-C_{3p} hereafter) ferroelectric phases, a zigzag phase boundary appeared from the upper side of the view field and moved down as the field increased [Fig. 2(a)]. Near the boundary region, $m/3$ -order ($m = 1$ and 2) RXS satellite reflections appeared in addition to the 1/2-order reflection in the applied field from ± 23 to $\pm 27\ \text{V}$ [Fig. 1(b1)]. It is noted that, at $\pm 27\ \text{V}$, when the measurement position was moved slightly into the field-induced Sm-C_{3p} phase, the 1/2-order reflection vanished and only the $m/3$ -order reflections remained. The ω -angular intensity profile [Fig. 1(b2)] indicated that the horizontal chevron, or “bookshelf,” structure was realized when the phase changed to Sm-C_{3p} .

Up to the $\pm 40\ \text{V}$ applied field, the $m/3$ -order satellite reflections and the bookshelf layer structure remained, as shown in Figs. 1(c1) and 1(c2), respectively. Around the $\pm 44\ \text{V}$ applied field, a phase boundary between the Sm-C_{3p} and Sm-C^* phases appeared in the view field [Fig. 2(b)] and the ω profile had a sharp peak [Fig. 1(d2)]. The $m/3$ -order satellite reflections were clearly observed, while the weak diffuse streak also appeared between the satellite and layer reflections [Fig. 1(d1)]. As seen in Fig. 2(b), the measurement point

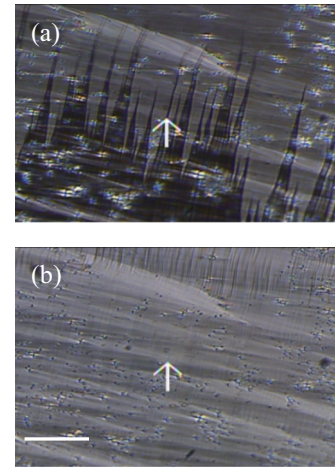


FIG. 2. (Color online) Sample photographs obtained at fields of (a) $\pm 27\ \text{V}$ and (b) $\pm 44\ \text{V}$ at 140°C . The white arrows indicate the measurement point. In (a), the upper region and lower regions correspond to the three-layer and two-layer periodicity phases, respectively, and the zigzag phase boundary in between. In (b), the region appearing in the topmost part of the photograph corresponds to the ferroelectric phase accompanied by the zigzag phase boundary, while other region appears to be the three-layer periodicity phase. The bar in (b) indicates a scale mark of $0.1\ \text{mm}$.

appears to still lie in the Sm-C_{3p} phase slightly outside the elongated zigzag phase boundary running almost parallel to the smectic layer direction. Further careful investigation showed that the diffuse streak consisted of weak spotty reflections in addition to $m/3$ -order reflections. Very close to or inside the phase boundary, only the streak was discernible. Above an applied field of over $\pm 45\ \text{V}$, the RXS peaks disappeared completely, suggesting a phase transition to the synclinic ferroelectric phase.

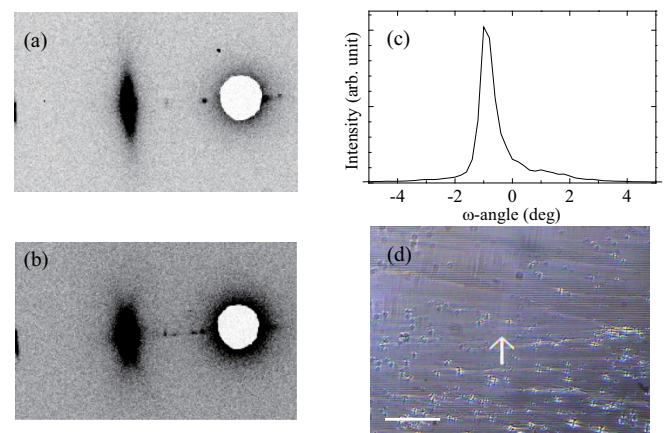


FIG. 3. (Color online) RXS patterns at applied fields of (a) $0\ \text{V}$ and (b) $\pm 26.5\ \text{V}$ at 144°C . Note that only the left parts of the diffraction patterns are shown: The strong first-order and weak second-order layer reflections are located around the center and the left edge, respectively. (c) The ω -angular profile and (d) a sample photograph at $\pm 26.5\ \text{V}$. A zigzag phase boundary with a weak contrast is seen at the left topmost region. The bar in (d) indicates a scale of $0.1\ \text{mm}$.

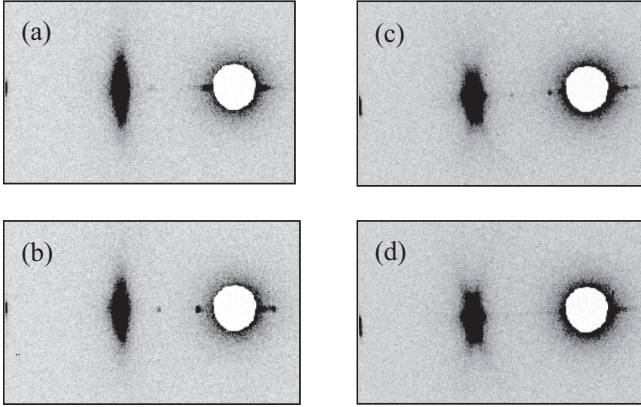


FIG. 4. RXS patterns at applied fields of (a) ± 3 V, (b) ± 6 V, (c) ± 20 V, and (d) ± 22 V at 145.1 °C.

At 144 °C [assigned as $\text{Sm-C}_A^*(q_T = 1/3)$ without the applied electric field], $m/3$ -order reflections appeared below ± 26.5 V [Fig. 3(a)]. Then the phase boundary between the Sm-C_{3p} and ferroelectric phases appeared [Fig. 3(d)] and the ω profile clearly showed the bookshelf (horizontal chevron) structure [Fig. 3(c)]. The RXS diffraction pattern again exhibited the spotty streak pattern [Fig. 3(b)] similar to Fig. 1(d1). In the Sm-C^* phase, the RXS peaks vanished.

At 145.2 °C [assigned as $\text{Sm-C}_A^*(q_T = 1/2)$], weak $m/4$ -order ($m = 1$ and 3) reflections appear up to ± 5 V [Fig. 4(a)], indicating a four-layer periodicity (assigned as Sm-C_{4p} hereafter), and then an $m/3$ -order reflection appeared up to ± 16 V [Fig. 4(b)]. Between ± 18 and ± 20 V, the spotty reflection first appeared between the $m/3$ -order reflections and the layer reflection [Fig. 4(c)], and then a weak streak remained at ± 22 V [Fig. 4(d)]. Above ± 24 V, the weak streak vanished in the synclinic ferroelectric phase.

At the higher temperature of 146 °C [also assigned as $\text{Sm-C}_A(q_T = 1/2)^*$], the Sm-C_{4p} phase appeared again at the low applied field [Fig. 5(a)], while the diffuse streak around the $m/3$ -order position appeared [Fig. 5(b)] at the higher field.

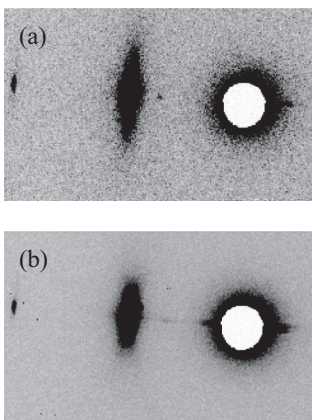


FIG. 5. RXS patterns at applied fields of (a) ± 1.5 V and (b) ± 6 V at 146 °C.

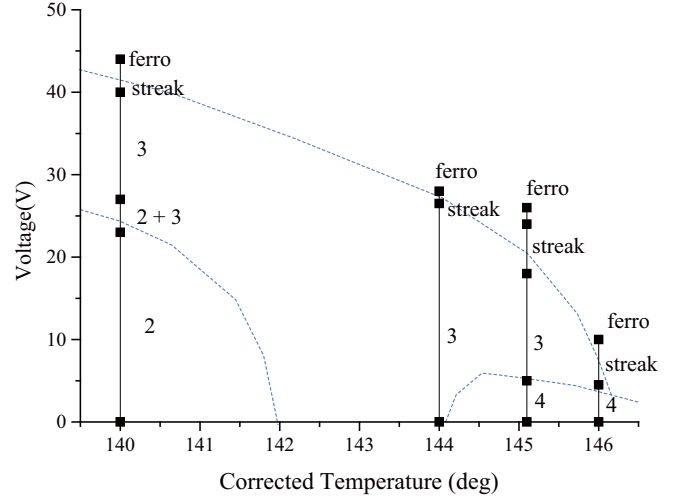


FIG. 6. (Color online) Phase diagram of temperature and applied voltage. The vertical lines show the temperatures at which the experiments were performed and the black squares denote the field-induced phase transition voltages. The integer values indicate the layer periodicity determined by RXS. “Streak” indicates diffuse scattering and the spotty patterns along the layer normal and “ferro” marks the region where no RXS satellite appears. The temperature was corrected according to polarized microscope images between different samples and different experimental runs. The phase boundaries are marked by dashed lines as a guide to the eyes.

IV. DISCUSSION

The field-induced phase transition shows the successive transition from the Sm-C_A^* to Sm-C^* phases. Figure 6 summarizes the experimental results as a function of temperature and applied voltage. The dependencies on the temperature and electric field of the various phases agree qualitatively with previous experimental results obtained by Hiraoka *et al.* [21] based on dielectric measurements, and results obtained by Shtykov *et al.* [22] from the pyroelectricity measurements and by Jaradat *et al.* [26] based on RXS. From the RXS measurements, two-, three-, and four-layer periodicity (Sm-C_{P2} , Sm-C_{P3} , and Sm-C_{P4}) phases were found to correspond to antiferroelectric $\text{Sm-C}_A^*(q_E = 0)$, ferroelectric $\text{Sm-C}_A^*(q_E = 1/3)$, and antiferroelectric $\text{Sm-C}_A^*(q_E = 1/2)$ phases, where $q_E = |[R] - [L]| / ([R] + [L])$, and $[R]$ and $[L]$ are the numbers of smectic layers with directors tilted to the right and to the left, respectively, in a unit periodicity [3,24].¹ In Fig. 6, the phase boundaries predicted from experimental results are also indicated by dashed lines.

Near the field-induced phase transition between the antiferroelectric $\text{Sm-C}_A^*(q_E = 0)$ and Sm-C_{3p} phases, $1/2$ - and $m/3$ -order reflections [Fig. 1(b1)] appeared simultaneously. Since no reflection other than $1/2$ and $m/3$ order was observed, both phases exist independently. Though

¹Though the q_E number has been once defined as a “fraction of R ” [2], according to the above definition, q_E is consistent with the q_T , i.e., $q_E = 0$ and $q_E = 1$ correspond to anticlinic and synclinic structures, respectively.

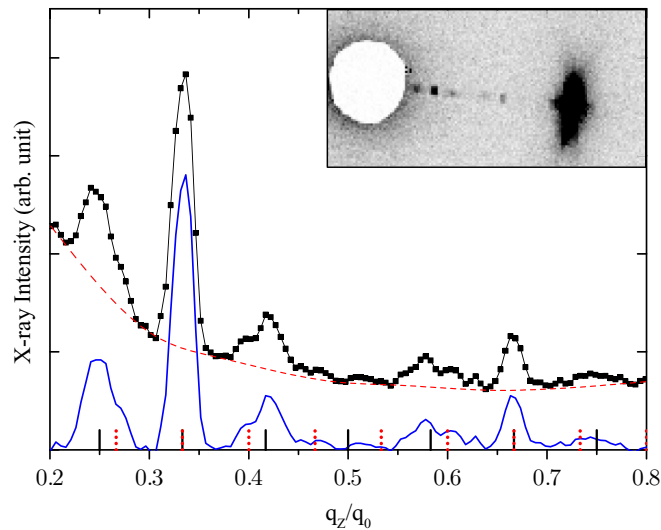


FIG. 7. (Color online) The intensity distribution along the layer normal as a function of the normalized scattering vector (q_z/q_0 , where $q_0 = 2\pi/d$ and d is a layer spacing) from the diffraction pattern obtained at 140°C and ± 44 V. The background (red) was subtracted from the original data (black squares and line). The black solid and pink dashed bars at the bottom correspond to the satellite position for the 12- and 15-layer periodicities, respectively. The inset photograph is horizontally reversed to agree with the graph.

the positional dependence of the reflection pattern near the phase boundary was not clear as the boundary lines moved slightly during the applied square-wave field cycle, the coexistence of the $1/2$ - and $m/3$ -order reflections can be due to the complicated geometrical phase boundary. However, the possibility of a microdomain with a size less than the beam size ($5\ \mu\text{m}$) cannot be excluded at present.

Near the field-induced phase transition between the Sm-C_{3p}^* and Sm-C^* phases from 140 to 145°C , a diffuse streak appeared in addition to the $m/3$ -order satellites. The streak at the lower applied field consists of spotty weak reflections. Figure 7

shows the integrated intensity profile in the radial direction from the diffraction pattern obtained at 140°C and ± 44 V. In addition to the strong $m/3$ -order reflections, $m/12$ -order (where $m = 3, 5, 7$, and 9) satellites are clearly observed, i.e., the 12-layer periodicity phase is realized under the application of the electric field. Furthermore, the side peaks of the $1/3$ and $2/3$ satellites, namely, the $(4 \pm 1)/12$ and $(8 \pm 1)/12$ satellites, appear to have shoulders that correspond to the $4/15$ and $6/15$ satellites of the 15-layer periodicity, even though the S/B ratio is not high enough to be reliable, compared to $m/12$ satellites. It is noted that such reflections are different from the mixture of three-layer and four-layer (or five-layer) periodicities, since the $5/12$ - and $7/12$ -order (or $4/15$ - and $6/15$ -order) reflections are unique to the 12-layer (or 15-layer) periodicity.

The satellite intensity pattern obtained from the neighboring regions (about a few tens of micrometers apart) with a relatively long measurement time (over several hours) was similar and stable. However, between different experimental runs and different sample cells, the intensity ratios between the satellite reflections were sometimes slightly different from those shown in Fig. 7. Even in those cases, however, peaks corresponding to the 12-layer periodicity were observed.

Though the long layer periodicity has been discussed theoretically [9,17,20] and experimentally [2,3,5,6,23,24], direct experimental evidence of a layer periodicity longer than six by the RXS measurement has yet to be reported, as far as the authors know. As the current satellites appeared in the transition region between the Sm-C_{3p}^* and Sm-C^* phases, they are considered to be related to the molecular orientational ordering near the phase transition. First, the possible orientational structure of the transition phase is discussed using the Ising model for simplicity. It is also assumed that these satellites arise from a single domain. From the $m/12$ reflections in Fig. 7, and taking into account that the Bragg angle was adjusted to the $1/3$ reflection, it can be seen that reflections for $m = 4$ and 8 are strong, while those for $m = 3, 5, 7$, and 9 are slightly weaker, and the $m = 6$ reflection is weakest.

By calculating RXS intensities for all possible Ising configurations according to the RXS theory [27,30], only two

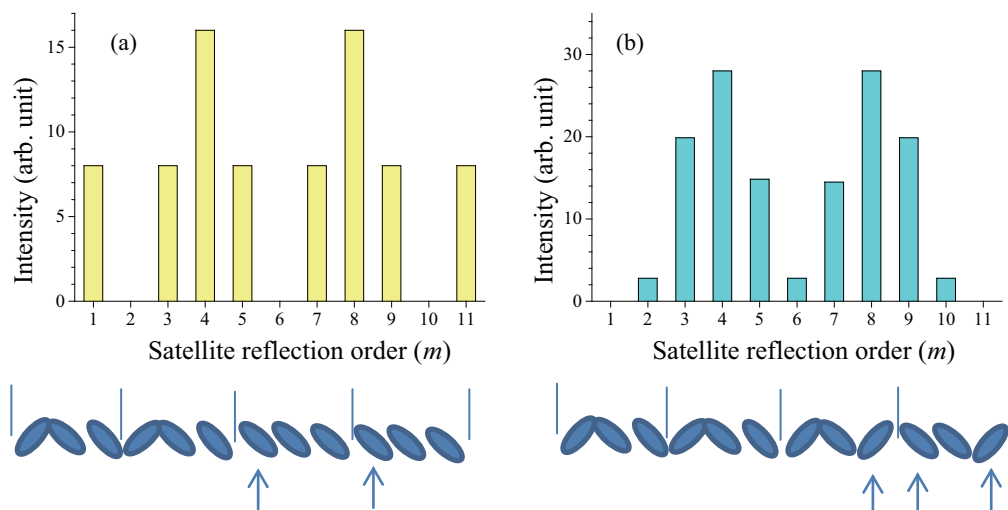


FIG. 8. (Color online) Calculated RXS satellite intensities based on two Ising models for the 12-layer periodicities shown in the lower panels, where m denotes a satellite order. The arrows indicate molecules which flip the tilt direction.

intensity patterns [Figs. 8(a) and 8(b)] for satellite reflection are plausible. The intensity pattern of Fig. 8(a) corresponds to the orientational structure which consists of two blocks of the ferroelectric three-layer structures and the six synclinc layers. A molecular tilt configuration is shown in the lower figure, and this occurs when only two molecules change the tilt direction (indicated by arrows) from an original ferroelectric three-layer structure. It is also noted that the ferroelectric three-layer periodicity blocks appear in succession. This orientational structure is $q_E = 2/3$, which is larger than $q_E = 1/3$ of the three-layer ferroelectric phase. It is noted that similar 12-layer structures consisting of three ferroelectric three-layer blocks and three synclinc layers produce almost the same satellite peak intensity ratio (strong $m/3$ -order satellites) as the original three-layer ferroelectric phase.

On the other hand, the orientational structure that produces the intensity pattern in Fig. 8(b) consists of four three-layer ferroelectric structures. In order to realize this configuration, three molecules should change their tilt direction against the applied field to create a new type of three-layer ferroelectric structure. Furthermore, the configuration shown in Fig. 8(b) is $q_E = 1/6$. As $q_E > 1/3$ is expected in the field-induced transition phase, the orientational structure shown in Fig. 8(b) is not reasonable.

When the 15-layer periodicity in addition to the 12-layer periodicity is assumed and the $m/15$ -order reflections for $m = 5$ and 10 are strong and those for $m = 4, 6, 9,$ and 11 are relatively weak, a few calculated satellite intensity patterns are likely to reproduce the experimental results. Orientational structures consisting of two to four ferroelectric three-layer periodicity blocks and synclinc layers for the other remaining layers are possible candidates, though the counting statistics was insufficient for further quantitative discussion.

From the above analyses, it is proposed that the three-layer periodicity structure is gradually replaced by the synclinc ferroelectric structure in the field-induced transition region. With further increases of the number of synclinc layers, i.e., when one three-layer periodicity ferroelectric layer remains in the surrounding synclinc structures, the reflections show equal weak intensity peaks at each $m/12$ position, since only one molecule tilts to the opposite direction every 12 layers. At this final stage, the reflection pattern can be observed as a diffuse streak.

Periodicities of longer than 15 were not resolved in these experimental results. On the other hand, for shorter periodicities, the nine-layer periodicity with two three-layer periodicity blocks and three synclinc layers and the six-layer periodicity with one three-layer ferroelectric block and three synclinc layers are possible candidates, but they were not observed. The intensity pattern of the RXS satellites often shows a satellite intensity ratio that is different from Fig. 7, when an electric field with a magnitude just below the phase transition to Sm-C* is applied. The various reflection intensity ratios can be simulated by a molecular orientation similar to Fig. 8(b), provided that the ferroelectric three-layer block with a molecular sequence is realized. The origin of these orientational configurations is not clear; it might be caused by the layer ordering defect, or by the fluctuation of the mechanism for creating the three synclinc layers.

Though the Ising model is rationalized due to the high applied field, when the calculation is extended to a distorted

clock model, the intensity ratio between various satellite orders changes, depending on the distortion degree and the azimuthal angle of the tilted smectic. When the intensity ratio is averaged over the azimuthal angle of the distorted structure, however, it is found that the intensity ratio obtained from the simple Ising model can be used as a guideline for discussing the orientational configuration. For instance, the distorted clock model corresponding to the Ising model of Fig. 8(a) yields a similar satellite intensity ratio as the Ising model itself, even though the relative intensities between the satellite peaks are slightly different.

The transition phase, which has a layer periodicity of greater than 12 layers, was observed. The long periodicity phase has been discussed in relation to the Sm-C α^* phase which typically appears between Sm-A and Sm-C* and is considered to have a short-pitch helical structure [10,11] with a few layers to ten-layer pitches. The phase sequence and the origin of the phase transition are different from the present field-induced transition phase. Furthermore, the RXS peak of the helical structure typically consists of a strong first-order satellite reflection and the helical pitch depends on the temperature in the Sm-C α^* phase [11], while no incommensurate first-order satellite was observed in the present experiment. Though recently intermediate phases which include the long periodicity phases have been discussed in relation to smooth transitions between the biaxial smectic subphase as a function of temperature [31], the molecular configurations should be quite different under the electric-field application.

The transition phase is expected to be a ferroelectric phase and to have $1/3 < q_E < 1$ as it appears between the three-layer periodicity phase ($q_E = 1/3$) and the synclinc phase ($q_E = 1$) due to the field-induced transition. For such an orientational configuration, a six-layer periodicity ($q_T = 2/3$) structure was discussed [14,15,18,23,24], although the six-layer periodicity alone cannot explain the extra satellite in the present experiment.

From these considerations, the transition phase does not agree with the phases that have already been proposed. It can be represented by the intermediate phase in which the ferroelectric order changes to the ferroelectric order by flipping the tilt direction of a few molecules. Although the origin of the stability of the long-range (12-layer) periodicity is not clear, the molecular structure which has two chiral carbons in both terminal groups may be effectively interacted in adjacent layers. Although this transition layer appears to be intrinsic to the field-induced transition, the stress caused by the cell structure might affect the generation of the transition phase. Further investigations using the different experimental setups and other types of samples are required to clarify the origin of this transition phase.

At 146 °C, the satellites corresponding to the three-layer structure, which appeared in a relatively narrow applied field range, showed a broad peak elongated along the radial direction [Fig. 5(b)]. The first-order layer reflection is the same as the ordinary reflection, so it does not result from variations in the thickness of the smectic layer due to the stress. Compared to the streaks appearing in the transition phase, as discussed above, it appears to be more concentrated around the $m/3$ -order reflections. This broad reflection might be caused by the short correlation length of the three-layer periodicity

domain in the ferroelectric phase, since in this temperature range the three-layer phase appeared in a relatively narrow applied field [2,3,21,22,26] so the stable large three-layer phase is difficult to grow.

V. CONCLUSION

In conclusion, the electric-field-induced phase transition of chiral smectic liquid crystals revealed a transition phase between the three-layer periodicity phase and the synclonic ferroelectric phase. The resonant microbeam x-ray scattering from the transition phase showed the diffuse streak and the spotty reflections. The spotty reflections were found to mainly be related to the 12-layer periodicity phase. The simple

Ising model calculation suggested that three-layer ferroelectric blocks ($q_E = 1/3$) changed into the synclonic block ($q_E = 1$).

ACKNOWLEDGMENTS

The authors would like to thank Professor Atsuo Fukuda for his valuable discussions and suggestions during the research. They would also like to thank Y. Ohtsuka and the staff of the Photon Factory for their help during the experiments. This work was carried out under the approval of the Photon Factory Advisory Committee (Proposals No. 2010G682, No. 2011G581, and No. 2012G635). This work was partly supported by the Grant-In-Aid for Scientific Research on Priority Area (A) (23246007) of the Ministry of Education, Culture Sports, Science and Technology.

-
- [1] S. T. Lagerwall, *Ferroelectric and Antiferroelectric Liquid Crystals* (Wiley, Weinheim, 1999).
- [2] A. Fukuda, Y. Takanishi, T. Isozaki, K. Ishikawa, and H. Takezoe, *J. Mater. Chem.* **4**, 997 (1994).
- [3] K. L. Sandhya, J. K. Vij, A. Fukuda, and A. V. Emelyanenko, *Liq. Cryst.* **36**, 1101 (2009).
- [4] A. D. L. Chandani, E. Gorecka, Y. Ouchi, H. Takezoe, and A. Fukuda, *Jpn. J. Appl. Phys.* **28**, L1265 (1989).
- [5] T. Isozaki, T. Fujikawa, H. Takezoe, A. Fukuda, T. Hagiwara, Y. Suzuki, and I. Kawamura, *Phys. Rev. B* **48**, 13439 (1993).
- [6] Yu. P. Panarin, O. Kalinovskaya, J. K. Vij, and J. W. Goodby, *Phys. Rev. E* **55**, 4345 (1997).
- [7] K. Itoh, M. Kabe, K. Miyachi, Y. Takanishi, K. Ishikawa, H. Takezoe, and A. Fukuda, *J. Mater. Chem.* **7**, 407 (1997).
- [8] M. Yamashita, *Ferroelectrics* **181**, 201 (1996).
- [9] M. Yamashita and S. Tanaka, *Jpn. J. Appl. Phys.* **37**, L528 (1998).
- [10] P. Mach, R. Pindak, A.-M. Levelut, P. Barois, H. T. Nguyen, C. C. Huang, and L. Furenid, *Phys. Rev. Lett.* **81**, 1015 (1998).
- [11] L. S. Hirst, S. J. Watson, H. F. Gleeson, P. Cluzeau, P. Barois, R. Pindak, J. Pitney, A. Cady, P. M. Johnson, C. C. Huang, A.-M. Levelut, G. Srajer, J. Pollmann, W. Caliebe, A. Seed, M. R. Herbert, J. W. Goodby, and M. Hird, *Phys. Rev. E* **65**, 041705 (2002).
- [12] N. W. Roberts, S. Jaradat, L. S. Hirst, M. S. Thurlow, Y. Wang, S. T. Wang, Z. Q. Liu, C. C. Huang, J. Bai, R. Pindak, and H. F. Gleeson, *Europhys. Lett.* **72**, 976 (2005).
- [13] P. D. Brimicombe, N. W. Roberts, S. Jaradat, C. Southern, S.-T. Wang, C.-C. Huang, E. DiMasi, R. Pindak, and H. F. Gleeson, *Eur. Phys. J. E* **23**, 281 (2007).
- [14] S. Wang, L. D. Pan, R. Pindak, Z. Q. Liu, H. T. Nguyen, and C. C. Huang, *Phys. Rev. Lett.* **104**, 027801 (2010).
- [15] Y. Takanishi, I. Nishiyama, J. Yamamoto, Y. Ohtsuka, and A. Iida, *Phys. Rev. E* **87**, 050503(R) (2013).
- [16] M. A. Osipov, A. Fukuda, and H. Hakoi, *Mol. Cryst. Liq. Cryst.* **402**, 9 (2003).
- [17] A. V. Emelyanenko and M. A. Osipov, *Phys. Rev. E* **68**, 051703 (2003).
- [18] P. V. Dolganov, V. M. Zhilin, V. K. Dolganov, and E. I. Kats, *Phys. Rev. E* **67**, 041716 (2003).
- [19] M. B. Hamaneh and P. L. Taylor, *Phys. Rev. Lett.* **93**, 167801 (2004).
- [20] P. V. Dolganov, V. M. Zhilin, and E. I. Kats, *J. Exp. Theor. Phys.* **115**, 1140 (2012).
- [21] K. Hiraoka, Y. Takanishi, K. Skarp, H. Takezoe, and A. Fukuda, *Jpn. J. Appl. Phys.* **30**, L1819 (1991).
- [22] N. M. Shtykov, J. K. Vij, R. A. Lewis, M. Hird, and J. W. Goodby, *Phys. Rev. E* **62**, 2279 (2000).
- [23] A. D. L. Chandani, N. M. Shtykov, V. P. Panov, A. V. Emelyanenko, A. Fukuda, and J. K. Vij, *Phys. Rev. E* **72**, 041705 (2005).
- [24] K. L. Sandhya, A. D. L. Chandani, A. Fukuda, S. Kumar, and J. K. Vij, *Phys. Rev. E* **87**, 062506 (2013).
- [25] L. S. Matkin, S. J. Watson, H. F. Gleeson, R. Pindak, J. Pitney, P. M. Johnson, C. C. Huang, P. Barois, A.-M. Levelut, G. Srajer, J. Pollmann, J. W. Goodby, and M. Hird, *Phys. Rev. E* **64**, 021705 (2001).
- [26] S. Jaradat, P. D. Brimicombe, C. Southern, S. D. Siemianowski, E. DiMasi, M. Osipov, R. Pindak, and H. F. Gleeson, *Phys. Rev. E* **77**, 010701 (2008).
- [27] A.-M. Levelut and B. Pansu, *Phys. Rev. E* **60**, 6803 (1999).
- [28] Y. Takanishi, I. Nishiyama, J. Yamamoto, Y. Ohtsuka, and A. Iida, *J. Mater. Chem.* **21**, 4465 (2011).
- [29] Y. Takanishi, Y. Ohtsuka, Y. Takahashi, and A. Iida, *Phys. Rev. E* **81**, 011701 (2010).
- [30] M. A. Osipov and M. V. Gorkunov, *Liq. Cryst.* **33**, 1133 (2006).
- [31] A. V. Emelyanenko and K. Ishikawa, *Soft Matter* **9**, 3497 (2013).